ACS OMEGA

Open Access

This article is licensed under CC-BY-NC-ND 4.0

http://pubs.acs.org/journal/acsodf

Article

Concerted Two-Proton-Coupled Electron Transfer from Piceatannol to Electrogenerated Superoxide in *N*,*N*-Dimethylformamide

Tatsushi Nakayama* and Bunji Uno

Cite This: *ACS Omega* 2024, 9, 24889−24898

Read Online

ACCESS | Metrics & More | Article Recommendations | Supporting Information

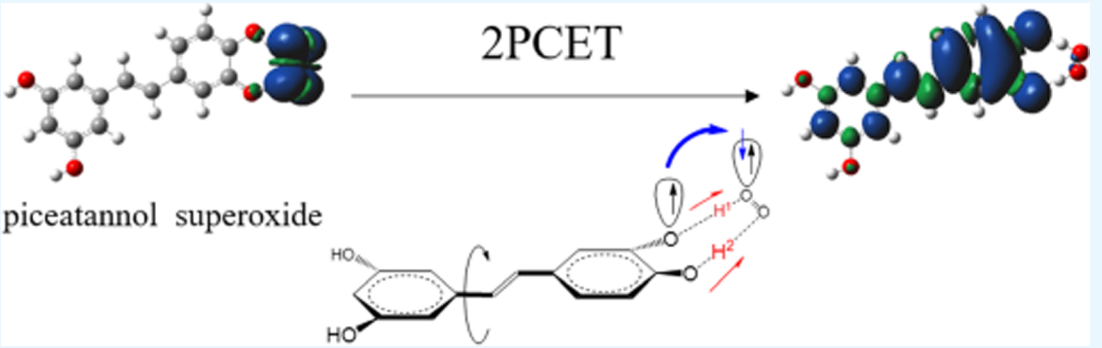

ABSTRACT: The reactivity of 4-[(*E*)-2-(3,5-dihydroxyphenyl)ethenyl]benzene-1,2-diol (piceatannol) toward electrochemically generated superoxide radical anion ($O_2^{\bullet-}$) was investigated using electrochemistry and in situ controlled-potential electrolytic electron spin resonance (ESR) measurements in *N*,*N*-dimethylformamide with density functional theory (DFT) calculations. The quasireversible cyclic voltammogram of dioxygen/$O_2^{\bullet-}$, modified in the presence of piceatannol, indicated that the electrogenerated $O_2^{\bullet-}$ was scavenged by piceatannol via proton-coupled electron transfer. Differences in the reactivities of piceatannol and 5-[(*E*)-2-(4-hydroxyphenyl)ethen-1-yl]benzene-1,3-diol (*trans*-resveratrol) toward $O_2^{\bullet-}$, originating from the presence of the benzene-1,2-diol (catechol) moiety, were observed in the voltammograms and ESR measurements. The electrochemical and computational results show that the reaction mechanism is a concerted two-proton-coupled electron transfer (2PCET) via the catechol moiety of piceatannol. The stilbene moiety of piceatannol kinetically promotes 2PCET via its catechol moiety. These findings indicate that piceatannol is a better $O_2^{\bullet-}$ scavenger than catechol and *trans*-resveratrol.

1. INTRODUCTION

4-[(*E*)-2-(3,5-Dihydroxyphenyl)ethen-1-yl]benzene-1,2-diol (piceatannol, $PiceH_4$) is a type of phenolic antioxidant, a stilbenoid,[1] and a phytoalexin[2] found in mycorrhizal and nonmycorrhizal roots of *Norway spruce*[3] and the seeds of the palm *Aiphanes horrida*[4] and *Gnetum cleistostachyum*.[5] Piceatannol is an analogue and also a metabolite of 5-[(*E*)-2-(4-hydroxyphenyl)ethen-1-yl]benzene-1,3-diol (*trans*-resveratrol, $RsvH_3$). In vitro studies have shown that piceatannol exhibits pharmacological effects against leukemia and non-Hodgkin's lymphoma, making it valuable as a multitarget molecule against various diseases.[6] In particular, piceatannol can scavenge the reactive oxygen species (ROS), potentially playing a therapeutic role as an antioxidant.[7,8] However, mechanistic insights into the therapeutic effects of piceatannol are yet fully to be demonstrated.

Chemical reactions including electron transfer (ET) to scavenge ROS such as the superoxide radical anion ($O_2^{\bullet-}$), hydroperoxyl radical ($HO_2^{\bullet}$), and hydroxyl radical ($HO^{\bullet}$) must be demonstrated to confirm the medicinal effects of piceatannol. Clarifying the ROS scavenging mechanism of piceatannol is a prerequisite to elucidate its medicinal effects, as ROS generated around lesions and inflammatory organs may directly cause several pathologies[7,8] Cordova-Gomez et al. investigated the peroxyl radical scavenging activity of piceatannol using density functional theory (DFT), compared it with that of *trans*-resveratrol—its structural analogue,[9] and concluded that piceatannol is a better peroxyl scavenger than *trans*-resveratrol. Piceatannol belongs to the stilbenoid group of polyphenols and possesses a benzene-1,2-diol (orthodiphenol, catechol) moiety and another phenolic ring linked to each other by an ethylene bridge with four hydroxyl groups (OH). Effective antioxidant activity is related to the quinone−hydroquinone π-conjugation characterized by the presence of ortho- or para-diphenolic OHs. The better ROS scavenging of

Received: February 22, 2024
Revised: May 1, 2024
Accepted: May 24, 2024
Published: May 31, 2024

© 2024 The Authors. Published by American Chemical Society

piceatannol compared with that of *trans*-resveratrol[10] is potentially due to the functionality of its catechol moiety, which can delocalize π-electrons with its resonance structure. However, the reactions of isolated $HO_2^\bullet$ and $HO^\bullet$ are difficult to observe experimentally because they are highly reactive. Consequently, deeper insights into the ROS scavenging mechanism of piceatannol remain unclear.

The antioxidant activities of polyphenol stilbenoids have been extensively studied using different assays and methodologies regarding the structure−activity or structure−property relationship related to the position and number of OHs,[10−14] and the electron-donating ability of stilbenoids has been discussed. Further, experimental data demonstrate that if the OH is scavenged or replaced by the methoxy group, the molecule loses its activity, suggesting that the OH is a proton donor and substituent with an electronic inductive effect.[14] Thus, ROS scavenging activity was evaluated using the bond dissociation energy and ionization potential of the OH representing the antioxidant property of the individual OHs and the entire molecule of stilbenoids. Consequently, several ROS scavenging mechanisms exist for piceatannol and other phenolic antioxidants, such as superoxide-facilitated oxidation,[15−17] single-electron transfer (SET), sequential proton-loss ET,[18] hydrogen-atom transfer (HAT), and proton-coupled electron transfer (PCET).[19−22] At present, the antioxidant mechanism is considered to involve ET and proton transfer (PT); thus, HAT involving PCET via hydrogen bonds (HBs) is a plausible ROS scavenging-antioxidant mechanism rather than SET.

We previously analyzed the PCET reaction between electrogenerated $O_2^{\bullet-}$ and phenolic antioxidants including catechols,[23−25] then, *trans*-resveratrol,[26] in *N*,*N*-dimethylformamide (DMF). Here, the $O_2^{\bullet-}$ cannot accept electrons from phenolic substrates because the $O_2^{\bullet-}$ is not so electrophilic; however, the $HO_2^\bullet$ (a protonated form of the $O_2^{\bullet-}$) is a strong oxidant. Thus, ET and PT from antioxidants/deprotonated anion to $O_2^{\bullet-}/HO_2^\bullet$ are closely related, potentially embodying the actual scavenging mechanism. Among them, concerted two-proton-coupled electron transfer (2PCET)—a type of PCET mechanism characterized by quinone−hydroquinone π-conjugation via the catechol moiety—is necessary for the efficient scavenging of $O_2^{\bullet-}$.[22−24] Conversely, *trans*-resveratrol scavenges $O_2^{\bullet-}$ through a PT forming $HO_2^\bullet$ followed by a concerted PCET via 4′OH, where the stilbene moiety is essential for the PCET.[26] Notably, piceatannol possesses both catechol and stilbene moieties, although it remains unclear how they contribute to $O_2^{\bullet-}$ scavenging via PCET.[9−11,13,27−29]

Herein, we investigated the reaction mechanism between piceatannol and electrogenerated $O_2^{\bullet-}$ in DMF by focusing on the role of the catechol and stilbene moieties of piceatannol. Next, we clarified which moiety primarily plays a functional role in the $O_2^{\bullet-}$ scavenging, showing the differences between piceatannol and *trans*-resveratrol. Accordingly, we reveal the mechanism of scavenging of piceatannol by the $O_2^{\bullet-}$ molecule, which is important for understanding its health benefits.

2. MATERIALS AND METHODS

2.1. Chemicals. Piceatannol (>98.0%), *trans*-resveratrol (>99.0%), 5-[(1*E*)-2-phenylethen-1-yl]benzene-1,3-diol (pinosylvin, >97.0%), 1,3-dimethoxy-5-[(*E*)-2-phenylethenyl]-benzene (3,5-dimethoxystilbene, >98.0%), and anhydrous DMF (>99.9%) for electrochemical and electrolytic electron spin resonance (ESR) spectral measurements purchased from Sigma-Aldrich Inc. (Tokyo, Japan) were used as received. We purchased tetrapropylammonium perchlorate (TPAP, >98.0%) from Tokyo Chemical Industry Co., Ltd. (Tokyo, Japan) and prepared for a supporting electrolyte as described previously.[30] Dinitrogen (N_2, 99.0%) and O_2 (99.0%) gases were purchased from Medical Sakai Co., Ltd. (Gifu, Japan). Ferrocene (Fc)—used as a reference for the electrochemical potential—was purchased from Nacalai Tesque Inc. (Kyoto, Japan) and used as received.

2.2. Electrochemistry and In Situ Controlled-Potential Electrolytic ESR Spectral Measurements. Electrochemical measurement was conducted in a three-electrode system comprising the working electrode: a 1.0 mm-diameter glassy carbon (GC), the counter electrode: a coiled platinum (Pt, 99.99%), and the reference electrode: a silver/silver nitrate ($Ag/AgNO_3$) containing tetrabutylammonium perchlorate (0.1 mol dm^{-3}) in an acetonitrile solution and $AgNO_3$ (0.01 mol dm^{-3}). A ferrocenium ion/ferrocene couple (Fc^+/Fc) was used for the calibration of the reference electrode. The working electrode was polished with alumina paste, rinsed with deionized water and acetone, and air-dried before the experiments. Data collection was conducted using an ECstat-301 electrochemical analyzer (EC-frontier Co., Ltd., Kyoto, Japan) at 25 °C (Supporting Information, Table S1). ESR spectra were obtained using a JES-X320 X-band spectrometer (JEOL Ltd., Tokyo, Japan). Controlled-potential electrolysis was performed in an ESR cell with a Pt working electrode (straight Pt wire with 0.5 mm-diameter sealed in a glass capillary) at 20 °C (Figure S1). Samples were prepared in a glovebox filled with dried N_2 gas to prevent moisture contamination of the samples. Weakly basic DMF was used as the solvent for the aprotic electrochemistry of the electrodes of the aprotic and low-phase $O_2/O_2^{\bullet-}$ to avoid free proton-derived electrode noise. DMF solutions containing TPAP (0.1 mol dm^{-3}) were saturated with O_2 by air-bubbling the gas for ca. 2−3 min. During the electrochemical and spectroelectrochemical measurements, O_2 gas was passed over the solutions for keeping a constant concentration (4.8×10^{-3} mol dm^{-3}).

3. THEORY AND CALCULATION

Solution-phase DFT calculations were conducted using three hybrid functionals: the Becke three-parameter Lee−Yang−Parr functional (B3LYP), the meta exchange-correlated functional (M06-2X),[31] and TPSSh,[32,33] implemented in the Gaussian 16 Program package.[34] We chose these functionals because they provide good geometries of the reactants, products, and transition states (TS) in PCET reactions.[35,36] The energies of the highest-occupied molecular orbital (HOMO) and the lowest-unoccupied molecular orbital (LUMO) were obtained from optimized geometry based on frontier orbital theory. The standard split-valence triple ζ basis sets augmented by the polarization d,p, and diffusion orbitals 6-311+G(d,p) were applied in the calculations. The polarized continuum model (PCM) was employed for the solvent contribution to the standard Gibbs free energies under the default settings of Gaussian 16. The standard Gibbs energies at 298.15 K were obtained from internal energies by using thermal correction, zero-point energies, and entropy. Population analysis using the natural bond orbital (NBO) technique was performed to obtain the numbers of electrons and spins.[37]

https://doi.org/10.1021/acsomega.4c01742
ACS Omega 2024, 9, 24889−24898

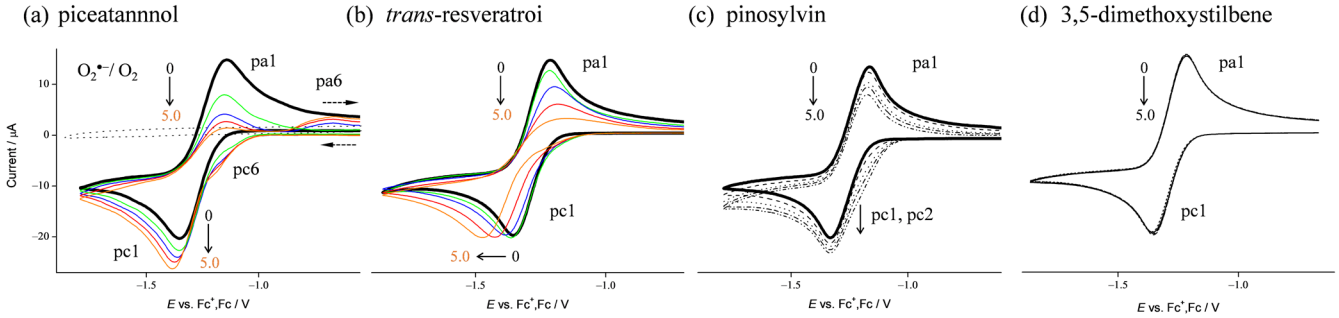

Figure 1. CVs of O_2 (4.8×10^{-3} mol dm^{-3}) with (a) piceatannol, (b) *trans*-resveratrol, (c) pinosylvin, and (d) 3,5-dimethyxystilbene in DMF containing TPAP (0.1 mol dm^{-3}); CV of (a) piceatannol without O_2 is shown as a control (dotted black line). CVs were recorded by using a GC working electrode at 0.1 V s^{-1}. Concentrations are (a, b) 0 (black), 1.0 (green), 2.0 (blue), 3.0 (red), and 5.0 (orange) and (c, d) 0, 1.0, 3.0, and 5.0 ($\times 10^{-3}$ mol dm^{-3}, the concentrations of stilbenoids are shown by arrows).

Chart 1. Structures of the Compounds Considered in this Study[a]

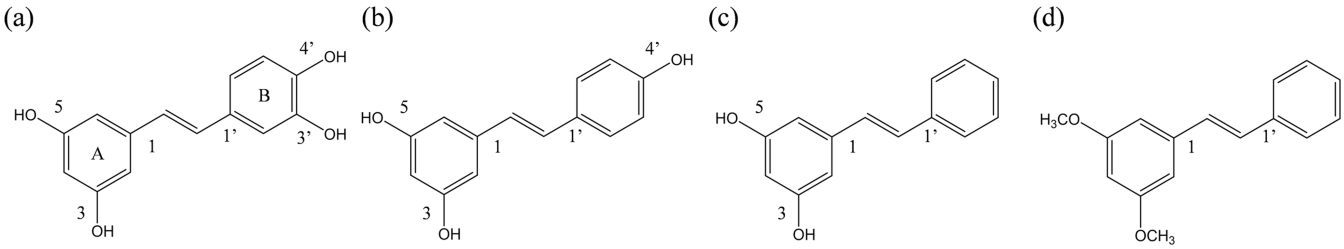

[a](a) 4-[(*E*)-2-(3,5-Dihydroxyphenyl)ethen-1-yl]benzene-1,2-diol (piceatannol), (b) 5-[(*E*)-2-(4-hydroxyphenyl)ethen-1-yl]benzene-1,3-diol (*trans*-resveratrol), (c) 5-[(1*E*)-2-phenylethen-1-yl]benzene-1,3-diol (pinosylvin), and (d) 1,3-dimethoxy-5-[(*E*)-2-phenylethenyl]benzene (3,5-dimethoxystilbene).

4. RESULTS AND DISCUSSION

4.1. Cyclic Voltammetry Analyses of $O_2/O_2^{\bullet-}$ in the Presence of Piceatannol. Cyclic voltammograms (CVs) of O_2 (4.8×10^{-3} mol dm^{-3}) with $PiceH_4$ (a), $RsvH_3$ (b), pinosylvin (c), and 3,5-dimethoxystilbene (d) were measured in DMF (Figure 1). The CVs shown in Figure 1b,c[26] are for comparison. In the CVs, O_2 is reduced by one electron generating $O_2^{\bullet-}$ in the cathodic scan and reoxidized to O_2 in the anodic scan (eq 1), where CV demonstrates a quasireversible redox couple of $O_2/O_2^{\bullet-}$ with cathodic/anodic peaks (pc1/pa1, bold lines in Figure 1). The quasireversible CVs of $O_2/O_2^{\bullet-}$ (eq 1) show no change in (d) but became irreversible in the presence of the phenolic stilbenoids as proton donors (a)−(c) at $0-5.0 \times 10^{-3}$ mol dm^{-3} concentrations, where CVs of the stilbenoids (Chart 1) without O_2 under bubbling N_2 gas demonstrated no peaks over the potential range (Figure 1a, dotted black line) because the stilbenoids are not electroreactive without deprotonation over most of the potential range (window) of DMF solvent (Supporting Information, Figure S2). Thus, the loss of reversibility of the CVs ($O_2/O_2^{\bullet-}$) was caused by an acid−base reaction, where $O_2^{\bullet-}$ (a Brønsted base) forms $HO_2^{\bullet}$ along the initial PT from the OH of acidic stilbenoids (eq 2).

Based on the loss of reversibility, the reactivity of piceatannol ($PiceH_4$) toward $O_2^{\bullet-}$ was greater than those of *trans*-resveratrol ($RsvH_3$) and pinosylvin. A prepeak (pc6 on pc1) and a prepeak (pc6) appear in Figure 1a in the presence of $PiceH_4$, which is different from those obtained with $RsvH_3$ (b). In addition, the appearance of the anodic peak with $PiceH_4$ differs from the overall reduction of O_2 to H_2O_2 observed with pinosylvin (Figure 1c, cathodic peak: pc2 on pc1), which involves the generation and subsequent heterogeneous reduction of $HO_2^{\bullet}$ (eq 3) showing a bielectronic CV.

$$O_2 + e^- \leftrightarrow O_2^{\bullet-}, \quad E^0_{Ox,Red} = -1.284 \text{ V vs. } Fc^+/Fc \tag{1}$$

$$PiceH_4 + O_2^{\bullet-} \rightarrow PiceH_3^- + HO_2^{\bullet}, \quad \text{the initial PT} \tag{2}$$

$$HO_2^{\bullet} + e^- \rightarrow HO_2^-, \quad E^0_{Ox,Red} = -0.4 \text{ to } -0.2 \text{ V vs. } Fc^+/Fc \tag{3}$$

Next, two CVs demonstrating the $O_2^{\bullet-}/HO_2^{\bullet}$ scavenging by $PiceH_4$ and $RsvH_3$ (Figure 1a,b) are compared. The cathodic curve with $RsvH_3$ considerably shifts to the negative-potential side (where its cathodic peak potential shifted from −1.355 to −1.474 V vs Fc^+/Fc), depending on the concentration of $RsvH_3$ ($0-5.0 \times 10^{-3}$ mol dm^{-3}). Conversely, CV with $PiceH_4$ showed no shift. This difference in the cathodic curves was due to the difference in the PCET mechanism, originating from the structures of $PiceH_4$ and $RsvH_3$. The shift in the presence of $RsvH_3$ is characteristic of the PCET among an extensive HB network formed between multiple OHs involving meta OH (3OH/5OH) on the stilbene moiety and $O_2/O_2^{\bullet-}$.[26] Therefore, the difference in the cathodic curve of $PiceH_4$ from that of $RsvH_3$ was possibly due to the 3′OH of $PiceH_4$, which comprised the catechol moiety reacting preferentially over the formation of HBs with 3OH/5OH.

To analyze the electrochemical mechanism shown in the CVs with $PiceH_4$ (Figure 1a), we further measured three types of CVs for the same solution containing O_2 and $PiceH_4$ using (a) a 1.0 V s^{-1} scan rate, (b) two cycles of continuous scanning, and (c) two cycles of continuous scanning at various scan rates (0.5−4.0 V s^{-1}) with the results (Supporting

https://doi.org/10.1021/acsomega.4c01742
ACS Omega 2024, 9, 24889−24898

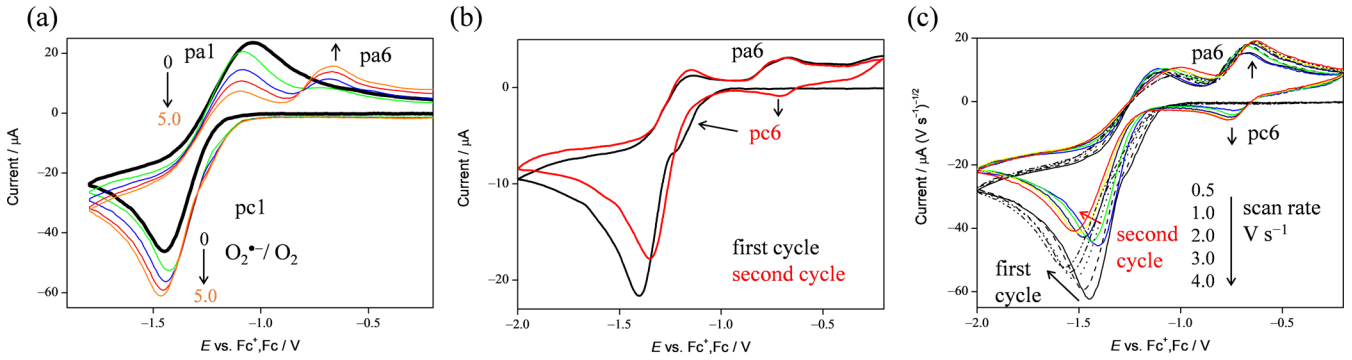

Figure 2. CVs of O_2 (4.8×10^{-3} mol dm^{-3}) with piceatannol in DMF containing TPAP (0.1 mol dm^{-3}), (a) at 1.0 V s^{-1} with piceatannol concentrations of 0 (black), 1.0 (green), 2.0 (blue), 3.0 (red), and 5.0 (orange) $\times 10^{-3}$ mol dm^{-3} (b) the first (black) and second (red) cycles of continuous scanning at 0.1 V s^{-1} with 5.0×10^{-3} mol dm^{-3} piceatannol concentration, and (c) two cycles of CVs (the first cycle: black, and the second cycle: colored) at various scan rates (0.5, 1.0, 2.0, 3.0, and 4.0 V s^{-1}, respectively) with 5.0×10^{-3} mol dm^{-3} piceatannol concentration, and currents (vertical axis) were shown after divided by the square roots of the scan rates. CVs were recorded by using a GC working electrode, and the concentrations (a) and scan rates (c) are indicated by arrows.

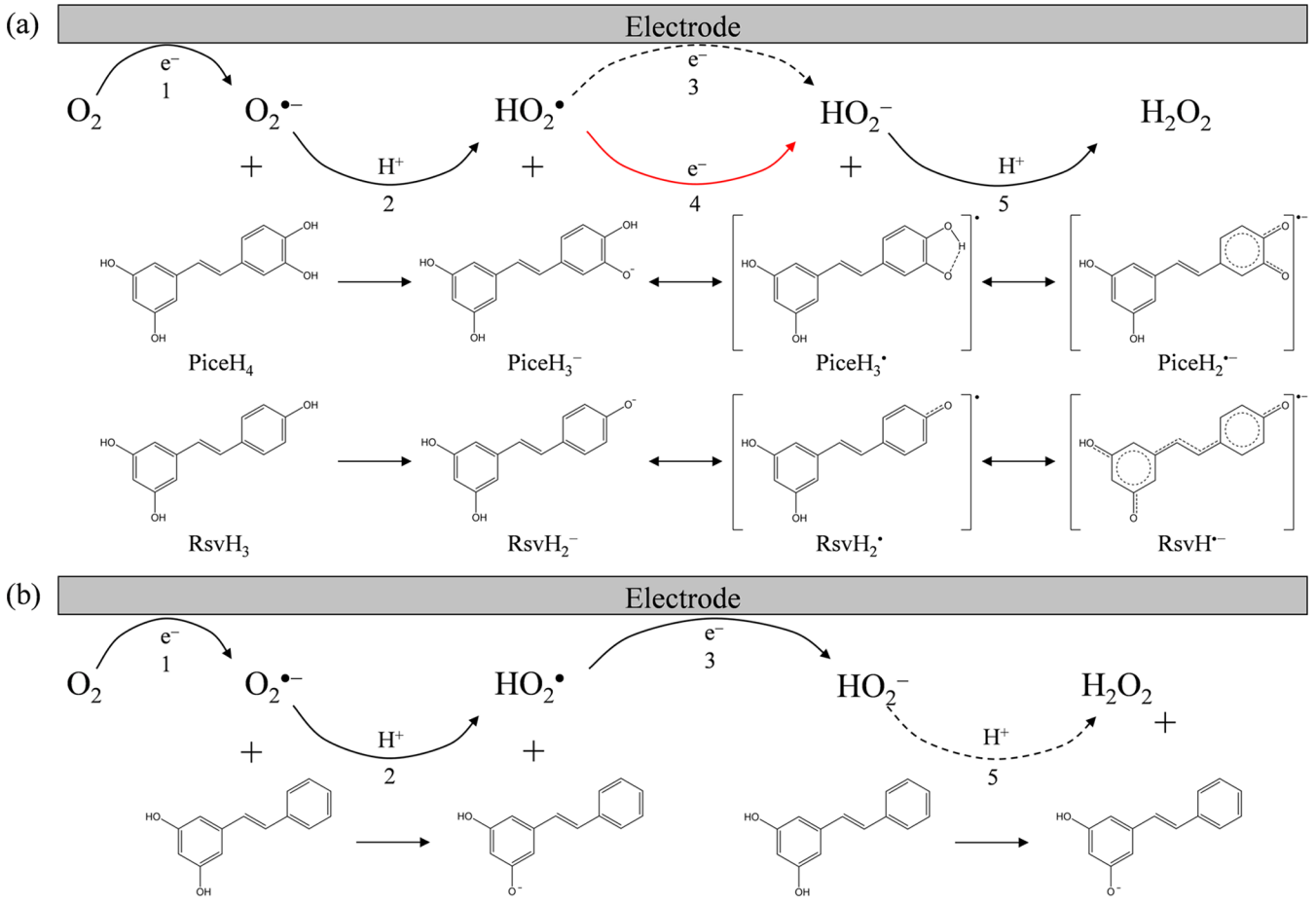

Figure 3. Electrochemical mechanisms of $O_2/O_2^{\bullet-}$ with (a) piceatannol ($PiceH_4$), *trans*-resveratrol ($RsvH_3$), and (b) pinosylvin in DMF; [1]one-electron reduction of $O_2/O_2^{\bullet-}$, [2]proton transfer from the acidic stilbenoid to $O_2^{\bullet-}$, [3]one-electron reduction of $HO_2^{\bullet}/HO_2^{-}$, [4]electron transfer from the stilbenoid anion to $HO_2^{\bullet}$ (red arrow), and [5]proton transfer to HO_2^{-}.

Information, Figure S3) divided by the square roots of the scan rates (Figure 2).

Figure 2a shows CVs at 1.0 V s^{-1} (scan rate) similar to those in Figure 1a (0.1 V s^{-1}), demonstrating a quasireversible redox couple of $O_2/O_2^{\bullet-}$ and the loss of reversibility with $PiceH_4$. The slight difference is that pa6 is clearer and larger in Figure 2a than in Figure 1a. Next, in the cathodic scan of the second cycle (red line) in Figure 2b, a peak is observed at the position corresponding to the redox couple with pa6, and the prepeak observed in the cathodic scan of the first cycle (pc6 on pc1) disappears. The potential of pa6 differed between the first and second cycles, indicating that pa6 was derived from the product of a series of PCET reactions triggered by the electrogeneration of $O_2^{\bullet-}$, i.e., the pc6/pa6 peaks plausibly originated from a reversible redox of a product of the PCET from $PiceH_4$ to $O_2^{\bullet-}$. The PCET involves the initial PT (eq 2)

https://doi.org/10.1021/acsomega.4c01742
ACS Omega 2024, 9, 24889−24898

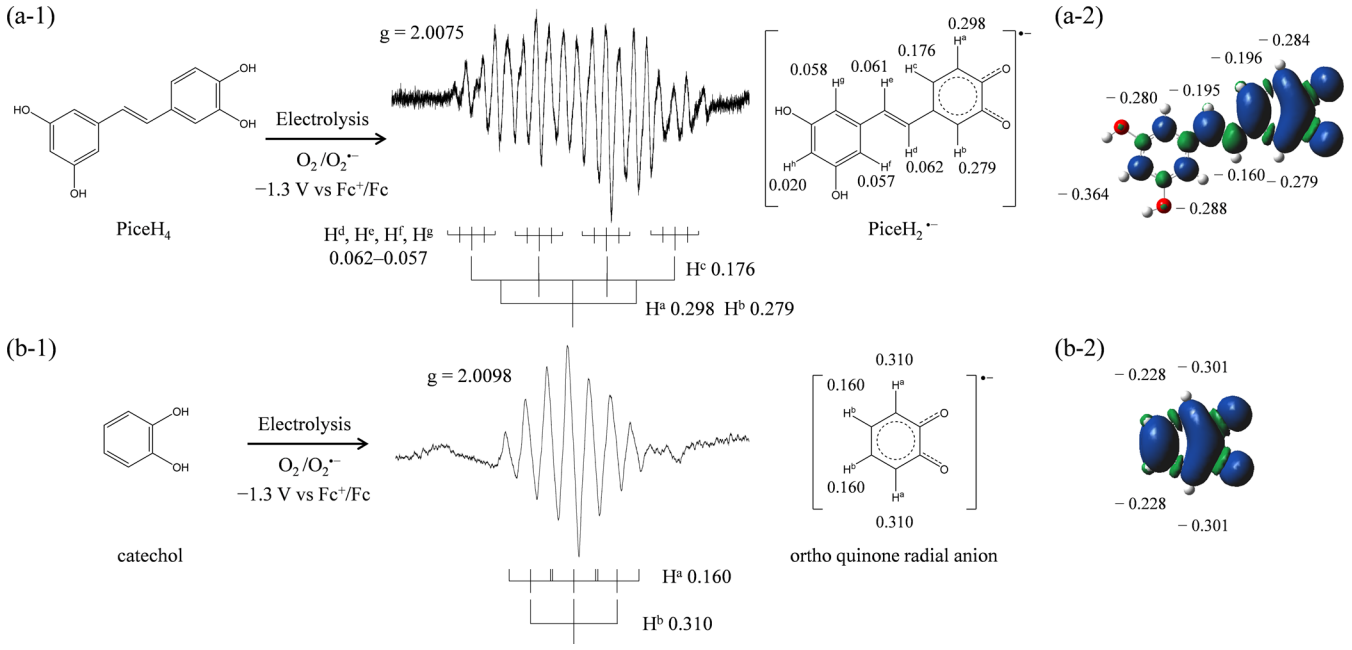

Figure 4. ESR spectra for O_2 (4.8×10^{-3} mol dm^{-3}) in DMF with (a-1) $PiceH_4$ and (b-1) catechol obtained by the in situ controlled-potential (−1.3 V vs Fc^+/Fc) electrolysis of solutions containing TPAP (0.1 mol dm^{-3}); radical structures with *g*-values and appropriate hyperfine coupling constants for hydrogen (a_H/mT) were obtained using simulations based on the measured spectra; spin distributions on (a-2) $PiceH_2^{\bullet-}$ and (b-2) catechol calculated using DFT-(U)B3LYP/PCM/6-311+G(d,p) with NBO analysis; charges distributed on carbons bonded to hydrogen are indicated.

followed by ET (eq 4) from the deprotonated anion ($PiceH_3^-$) to $HO_2^{\bullet}$, forming a substrate radical ($PiceH_3^{\bullet}$) and a hydroperoxyl anion (HO_2^-). In addition, Figure 2c demonstrates the effects of scan rates on the second cycle of CV. As the scan rate increases, the bielectronic cathodic peak (pc6 on pc1 in both the first and second cycles) becomes smaller because the slow diffusion of substances in the electrode surface usually limits the electrode process. Nevertheless, the pc6/pa6 couple in the second cycle becomes larger. These CV appearances with scan rate dependency demonstrated that the reversible redox (pc6/pa6) appeared in the second cycle scan derived from a quinoid radical as a product of the PCET. We speculated that a quinoid radical derived from the catechol moiety at the B ring of $PiceH_4$ was formed after the second PT (eq 5) for its chemical reversibility. Conversely, the electronic CV behavior was not observed in the presence of $RsvH_3$ (Figure 1b) owing to the ET scavenging $HO_2^{\bullet}$ and subsequent degradation of the generated radical.

$$HO_2^{\bullet} + PiceH_3^- \rightarrow HO_2^- + PiceH_3^{\bullet}, \quad \text{ET} \tag{4}$$

$$HO_2^- + PiceH_3^{\bullet} \rightarrow H_2O_2 + PiceH_2^{\bullet-}, \quad \text{the second PT} \tag{5}$$

Based on the CV results, the electrochemical mechanisms of $O_2/O_2^{\bullet-}$ with acidic stilbenoids (Figure 1a−c) are plausibly summarized in Figure 3, including eqs 1−5. The CV results recorded with $PiceH_4$ and $RsvH_3$ (Figure 1a,b) demonstrated the scavenging of the $O_2^{\bullet-}/HO_2^{\bullet}$ via PCET (Figure 3a), involving eqs 1, 2, 4, and 5. Conversely, the CV result with pinosylvin (Figure 1c) demonstrated the absence of $O_2^{\bullet-}/HO_2^{\bullet}$ scavenging (Figure 3b), showing the electrochemical electro processes of O_2/HO_2^- (eqs 1−3). Thus, the comparison revealed that the B ring (the mono phenolic moiety of $RsvH_3$ and the catechol moiety of $PiceH_4$) provided mechanistic insights into the $O_2^{\bullet-}/HO_2^{\bullet}$ scavenging via the PCET mechanism.

4.2. In Situ Controlled-Potential Electrolytic ESR Analyses of $O_2/O_2^{\bullet-}$ with Piceatannol. To confirm the differences in the PCET mechanisms from stilbenoids to $O_2^{\bullet-}$, the CV solutions (Figure 1a−d) under an applied potential of −1.3 V corresponding to the electrogeneration of $O_2^{\bullet-}$ (eq 1) were analyzed using ESR spectral measurements in an in situ electrolytic cell (Supporting Information, Figure S1). The ESR spectrum was obtained only with $PiceH_4$, implying that PCET involving PT and ET from $PiceH_4$ to $O_2^{\bullet-}$ occurred, forming a product radical (Figure 4a-1). Next, the hyperfine coupling constants for hydrogen (a_H/mT) were simulated based on the measured ESR spectra. Further, spin distributions on the structures of the product radicals ($PiceH_2^{\bullet-}$) were calculated by using DFT-(U)B3LYP/PCM/6-311+G(d,p) with NBO analysis (a-2). In addition, charges on carbons bonded to hydrogen are indicated. Based on the calculation results, the simulated a_H values were assigned to the hydrogen of $PiceH_2^{\bullet-}$ (H^a−H^h: 0.298, 0.279, 0.176, 0.062, 0.061, 0.058, 0.057, and 0.001 mT).

Similarly, the ESR spectrum with a_H of 0.31 and 0.16 mT was obtained for catechol, and then the ortho quinone radical was assigned to its product radical using the simulation (Figure 4b-1) and DFT calculation (b-2). The fact that only these two ESR spectra were detected suggests that the catechol moiety (B ring) of $PiceH_4$ plays an important role in the PCET. Interestingly, spins are primarily distributed in the B ring (H^a−H^c) and throughout the molecule of $PiceH_2^{\bullet-}$, as shown in the ESR results. In the CVs shown in Figure 2, a reversible redox couple (pc6/pa6) derived from the product appeared, indicating that the product was a quinoid radical ($PiceH_2^{\bullet-}$) derived from the catechol moiety of the B ring and suggesting that the reaction site of PCET was influenced by the structural differences between $PiceH_4$ and $RsvH_3$. In addition, the a_H

https://doi.org/10.1021/acsomega.4c01742
ACS Omega 2024, 9, 24889−24898

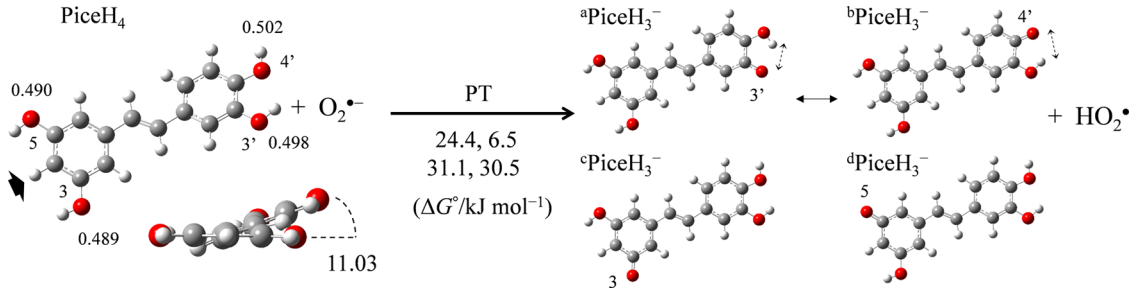

Figure 5. Optimized structures of piceatannol ($PiceH_4$) and deprotonated anions ($^aPiceH_3^-$, $^bPiceH_3^-$, $^cPiceH_3^-$, and $^dPiceH_3^-$) along the proton transfer from its hydroxyl group (3OH, 5OH, 3′OH, and 4′OH) to $O_2^{\bullet-}$ in DMF, calculated using DFT-B3LYP/PCM/6-311+G(d,p); charges distributed on the four OH protons of $PiceH_4$ obtained using NBO analysis and ΔG^0s (kJ mol^{-1}, 298.15 K) of proton transfer are indicated.

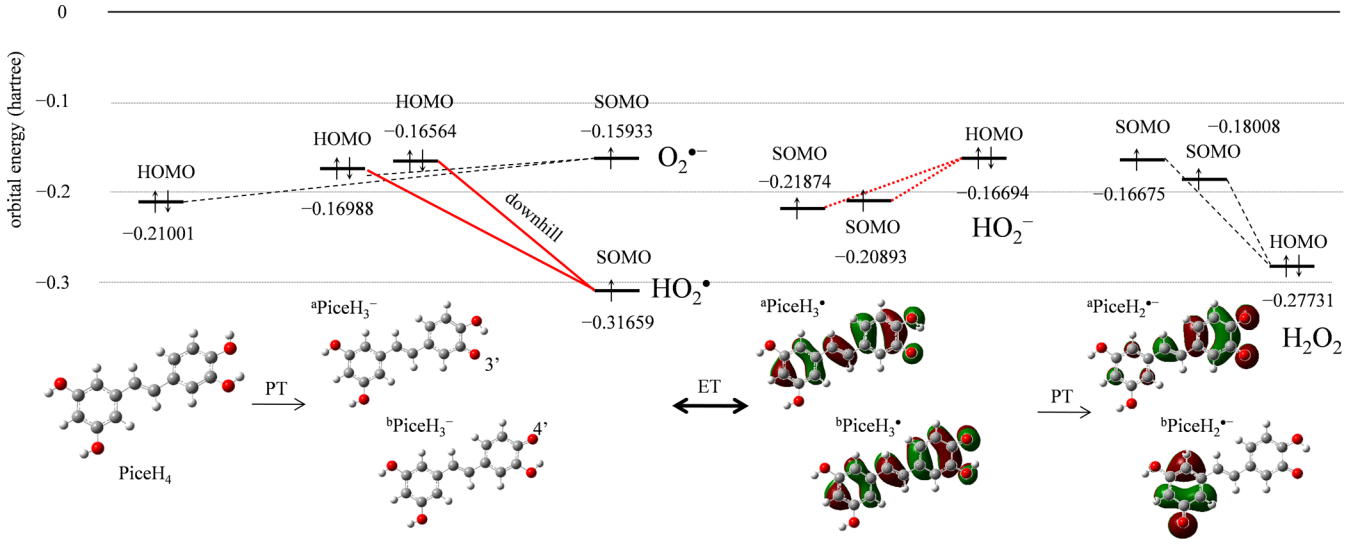

Figure 6. Changes in HOMO−LUMO energies (Hartree/a.u.) during proton-coupled electron transfer between piceatannol ($PiceH_4$) and $O_2^{\bullet-}$ in DMF were calculated using DFT-B3LYP/PCM/6-311+G(d,p).

values obtained from the ESR spectrum were assigned to the hydrogen on another phenolic ring (A ring, H^f−H^h) and the linked ethylene bridge (stilbene double bond, H^d and H^e), clarifying that the coplanar stilbene moiety contributes to PCET at the catechol moiety. A similar role of the stilbene moiety in contributing to the PCET reaction is expected to occur in the $RsvH_3$ molecule, although it was suggested that its product radical, generated via PCET, decomposes upon a subsequent reaction (the ESR spectrum was undetectable).

Analogous to the CV and ESR results, $RsvH_3$ and $PiceH_4$ scavenge the electrogenerated $O_2^{\bullet-}$ via PCET based on their structural characteristics as polyphenol stilbenoids. To the best of our knowledge, this is the first report of the ESR spectrum of the piceatannol radical, which was made observable using an in situ spectroelectrochemical system in a well-dried aprotic DMF solution. In addition, a difference in the stabilities of their product radicals ($PiceH_2^{\bullet-}$ and $RsvH^{\bullet-}$) based on the involvement of the catechol moiety implies a difference in the details of the PCET mechanism.

4.3. DFT Analyses of PCET from $PiceH_4$ to $O_2^{\bullet-}$. *4.3.1. Optimized Structures of $PiceH_4$ and Its Deprotonated Anion.* To elucidate the mechanism of PCET between $PiceH_4$ and $O_2^{\bullet-}$ in DMF, DFT calculations were conducted using the B3LYP, M06-2X, and TPSSh hybrid functionals with the PCM method. We focus on the B3LYP results below unless otherwise noted because the three functionals showed similar results. First, the stable conformations of $PiceH_4$ (Supporting Information, Figure S4) and the structures of its anions ($^aPiceH_3^-$, $^bPiceH_3^-$, $^cPiceH_3^-$, and $^dPiceH_3^-$) after the initial PT were obtained by energy scanning of the dihedral angle around the four OHs and stilbene moiety (Tables S2 and S3). Figure 5 shows the optimized structures and Gibbs free energy changes (ΔG^0/kJ mol^{-1}, 298.15 K) along the initial PT (M06-2X and TPSSh results are shown in the Supporting Information, Figure S5). Then, charge distributions on the OH protons of $PiceH_4$ obtained using NBO analysis were indicated.

The optimized structures revealed that the dihedral angle of the two phenolic rings around the stilbene double bond of $PiceH_4$ is 11.03°, and its anion has an approximately planar structure in DMF. Comparing the charges on the four OH protons of $PiceH_4$ (3′OH: 0.498, 4′OH: 0.502, 3OH: 0.489, and 5OH: 0.490), the acid−base reactivities of proton (acidity) slightly higher at 3′OH and 4′OH in the catechol moiety than those at 3OH and 5OH. Similarly, the ΔG^0s indicate that the deprotonation at 3′OH and 4′OH forming $^aPiceH_3^-$ (24.4) and $^bPiceH_3^-$ (6.5) is more plausible than that at 3OH and 5OH forming $^cPiceH_3^-$ (31.1) and $^dPiceH_3^-$ (30.5), respectively, owing to the intramolecular hydrogen bond at two catechol oxygens (3′OH−H−4′O) in the anions. According to these calculations, PT was initiated at 3′OH or 4′OH, which forms $^aPiceH_3^-$ or $^bPiceH_3^-$, respectively.

4.3.2. Changes in HOMO−LUMO Relation during PCET between $PiceH_4$ and $O_2^{\bullet-}$. The mechanistic analysis of PCET

https://doi.org/10.1021/acsomega.4c01742
ACS Omega 2024, 9, 24889−24898

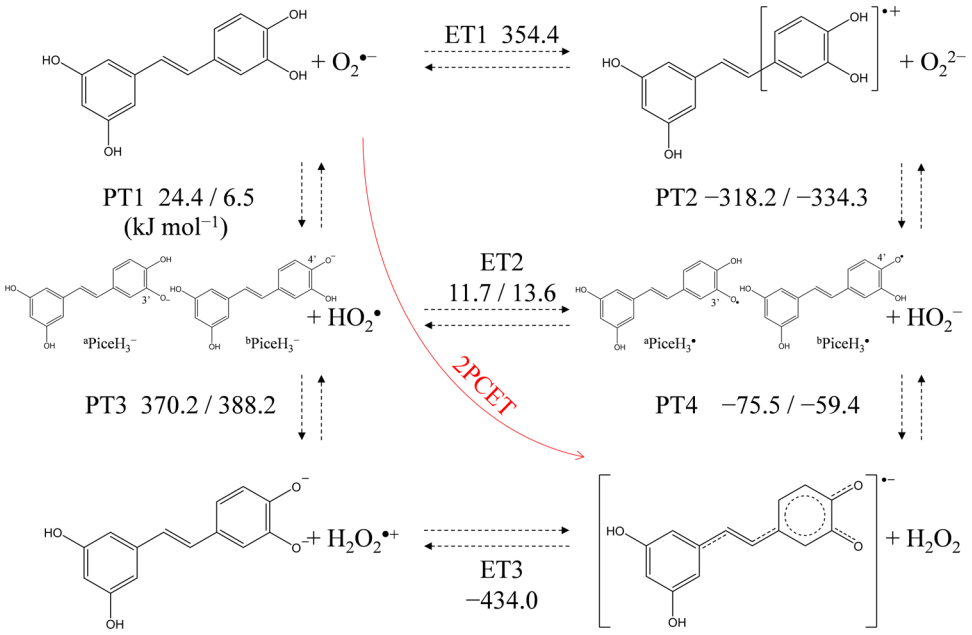

Figure 7. Equilibrium scheme of one electron transfer (ET1−ET3) and two proton transfers (PT1−PT4) from piceatannol ($PiceH_4$) to $O_2^{\bullet-}$ in DMF; ΔG^0s (kJ mol^{-1}, 298.15 K) were calculated using DFT-(U)B3LYP/PCM/6-311+G(d,p).

Table 1. ΔG^0 Values (kJ mol^{-1}, 298.15 K) of Proton-Coupled Electron Transfer from Piceatannol ($PiceH_4$), *trans*-Resveratrol ($RsvH_3$), Pinosylvin, to $O_2^{\bullet-}$ in DMF, Calculated Using B3LYP, M06-2X, and TPSSh Functionals, with the PCM/6-311+G(d,p) Basis Set

	stilbenoids	[a]PT1	PT2	PT3	PT4	ET1	ET2	ET3	[b]total
B3LYP	[c]$PiceH_4$	18.9	−318.2	370.2	−75.5	348.9	11.7	−434.0	−44.8
	[c]$RsvH_3$	30.6	−310.4	317.3	−45.8	356.6	15.5	−347.6	0.4
	Pinosylvin	37.3	−314.0	349.5	−66.7	380.6	29.2	−386.9	−0.1
M06-2X	[c]$PiceH_4$	28.3	−347.4	380.6	−96.2	412.6	36.7	−440.0	−31.0
	[c]$RsvH_3$	32.0	−313.8	314.7	−79.3	407.1	61.3	−332.7	14.0
	Pinosylvin	32.3	−341.6	353.0	−75.6	436.4	62.4	−366.3	19.1
TPSSh	[c]$PiceH_4$	11.7	−337.6	369.8	−61.4	365.0	15.6	−415.5	−34.0
	[c]$RsvH_3$	32.0	−289.8	299.9	−76.7	361.5	39.6	−336.9	−4.9
	Pinosylvin	29.9	−313.4	342.4	−75.0	386.2	42.8	−374.6	−2.3

[a]Proton transfer (PT1−PT4) and electron transfer (ET1−ET3). [b]The total values correspond to the sum of those for one ET and two PTs. [c]PT1 and PT2 occur at 3′OH of $PiceH_4$ and 3OH of $RsvH_3$, and PT3 and PT4 occur at 4′OH.

between $O_2^{\bullet-}$ and $PiceH_4$ was conducted using frontier molecular orbital analysis (Figure 6). The HOMO−LUMO (hartree/a.u.) relation changes during the PCET (M06-2X and TPSSh results are shown in the Supporting Information, Figure S6). Some reactant species, $PiceH_4$, $PiceH_3^-$, $O_2^{\bullet-}$, and $HO_2^{\bullet}$, coexist in the experimental solutions after the initial PT. The HOMO energies of $PiceH_4$ (−0.21001) and its anions ([a]$PiceH_3^-$: −0.16988, [b]$PiceH_3^-$: −0.16564) were much higher than the SOMO energy of $HO_2^{\bullet}$ (−0.31659), indicating that $HO_2^{\bullet}$ rather than $O_2^{\bullet-}$ (−0.15933) was the electron acceptor. Meanwhile, CV revealed that $PiceH_4$ scavenged $O_2^{\bullet-}$ and $HO_2^{\bullet}$ formed after the initial PT (Figure 1a). Therefore, $PiceH_3^-$ was the electron donor, as shown in the downhill energy relation (bold red lines). The HOMO−LUMO energies changed during PT from $PiceH_4$ to $O_2^{\bullet-}$, forming $PicesH_3^-$ and $HO_2^{\bullet}$, respectively. Moreover, the HOMO−LUMO relation between the products (i.e., [a]$PiceH_3^{\bullet}$/[b]$PiceH_3^{\bullet}$ and HO_2^-) is upset after the subsequent ET (red dotted lines), suggesting that reverse ET proceed. However, the HOMO (−0.27731) of H_2O_2 is lower than that of HO_2^- (−0.16694), indicating that the second PT prevents the reverse ET. Hence, the second PT predominantly determined the direction of ET. This HOMO−LUMO relation is similar whether the second PT occurs from 4′OH forming [a]$PiceH_2^{\bullet-}$ (−0.16675) or from 3OH/5OH forming [b]$PiceH_2^{\bullet-}$ (−0.18008). As a result of the frontier molecular orbital analysis, the net PCET between the $O_2^{\bullet-}$ and $PiceH_4$ involved one ET and two PTs, resulting in the formation of H_2O_2.

4.3.3. Gibbs Free Energy Changes in PCET from $PiceH_4$ to $O_2^{\bullet-}$. ΔG^0s (kJ mol^{-1}, 298.15 K) along the PCET were calculated by using the vibrational frequency calculation combined with the PCM method for the thermodynamically mechanistic analysis of the scavenging of the $O_2^{\bullet-}$ by $PiceH_4$ in DMF (Table S4). Figure 7 shows the redox equilibrium scheme and the ΔG^0s of PCET involving one ET and two PTs from $PiceH_4$ to $O_2^{\bullet-}$, calculated using the B3LYP/PCM/6-311+G(d,p) method (M06-2X and TPSSh results are shown in the Supporting Information, Figure S7). The ΔG^0s of the individual reactions of the components in Figure 7, ET1−ET3 and PT1−PT4, are the main drivers of the sequential pathway. Because ET1 (354.4) was strongly endergonic, PT1 (24.4, 6.5) predominantly formed [a]$PiceH_3^-$/[b]$PiceH_3^-$ and $HO_2^{\bullet}$. At the

https://doi.org/10.1021/acsomega.4c01742
ACS Omega 2024, 9, 24889−24898

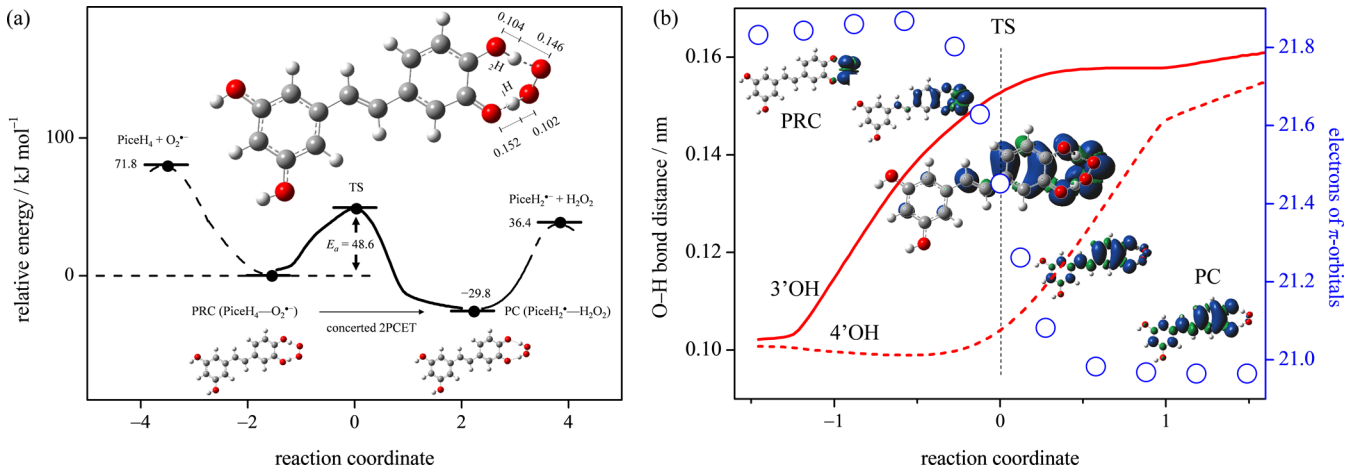

Figure 8. (a) Energy profile (kJ mol^{-1}, 298.15 K) along the formation of prereactive complex (PRC, PiceH$_4$—O$_2^{\bullet-}$), intrinsic reaction coordinate of two-proton-coupled electron transfer in the PRC from piceatannol (PiceH$_4$) to O$_2^{\bullet-}$, and dissociation of product complex (PC, PiceH$_2^{\bullet-}$—H$_2$O$_2$) in DMF with the structures of the PRC, transition state (TS), and the PC; (b) changes in the O—H bond distance (3′OH: red bold line, 4′OH: red dotted line, nm) and the number of π-electron of PiceH$_4$ (blue open circles) with the spin distributions; calculations were performed using the DFT-(U)B3LYP/PCM/6-311+G(d,p) with the NBO analyses.

bottom of the panels in Figure 7, PT3 (370.2, 388.2) and ET2 (11.7, 13.6) were endogenous; therefore, the sequential pathway was unlikely to proceed. Thus, the only feasible pathway is a concerted PCET involving one ET and two PTs in one step, where intermediates are not generated. We refer to this pathway as the 2PCET reaction.[23−25,36] Notably, 2PCET must occur in a one-kinetic process among an HB complex formed from the catechol moiety of PiceH$_4$ to form O$_2^{\bullet-}$.

The ΔG^0 values of the PCET pathways of PiceH$_4$, RsvH$_3$, and pinosylvin were calculated by using B3LYP, M06-2X, and TPSSh functionals for comparison (Table 1). The sum of the ΔG^0s of the one ET and two PTs is an energetic driving force of PCET, although that cannot embody it if PCET occurred along a pathway involving an infeasible single PT/ET. Along the plausible sequential pathway based on the electrochemical results (Figure 1), the ΔG^0s of PT1 and ET2 for PiceH$_4$ or RsvH$_3$ were endergonic obtained using each functional. Thus, 2PCET was the only feasible pathway for each compound (Table 1). However, the ΔG^0s of the total values for pinosylvin (B3LYP: −0.1, M06-2X: 19.1, TPSSh: −2.3) were similar to those for RsvH$_3$ (0.4, 14.0, and −4.9) but larger than those for PiceH$_4$ (−44.8, −31.0, and −34.0, respectively), inconsistent with the electrochemical results. Thus, the ΔG^0 values alone cannot explain the higher reactivities of PiceH$_4$ than those of RsvH$_3$ and pinosylvin toward electrogenerated O$_2^{\bullet-}$ observed in the loss of reversibility (Figure 1).

4.3.4. Reaction Coordinates and Potential Energy Surfaces of PCET from Piceatannol to O$_2^{\bullet-}$. The potential energy surfaces were scanned using the DFT-(U)B3LYP/PCM/6-311+G(d,p) combined with NBO calculations to gain mechanistic insights into the PCET of O$_2^{\bullet-}$/HO$_2^{\bullet}$ scavenging by PiceH$_4$. Three elementary steps were assumed during the reaction in DMF: (i) formation of a prereactive complex (PRC) via HBs from free reactants, (ii) 2PCET via a TS forming a product complex (PC), and (iii) PC dissociation yielding the free products. First, we performed structural optimization of feasible PRCs formed with a combination of free reactants, namely, O$_2^{\bullet-}$, HO$_2^{\bullet}$, PiceH$_4$, and PiceH$_3^-$ (step (i)). Among these, a PRC comprising PiceH$_4$ and O$_2^{\bullet-}$ (PiceH$_4$—O$_2^{\bullet-}$)—formed via the catechol moiety—was more stabilized (71.8 kJ mol^{-1}) by two HBs than the other PRCs. Next, the intermediate complex, PC, and TS, along with the subsequent PCET, were scanned (Table S5). In addition, some PRCs comprising PiceH$_4$ and HO$_2^{\bullet}$ via a single HB at each OH (3OH, 5OH, 3′OH, and 4′OH) were scanned, potentially leading to subsequent reactions. Consequently, only a PRC formed between the catechol moiety of PiceH$_4$ and O$_2^{\bullet-}$ (PiceH$_4$—O$_2^{\bullet-}$) could form a PC (PiceH$_2^{\bullet-}$—H$_2$O$_2$) through the 2PCET. And, a TS (step (ii)) and an intrinsic reaction coordinate (IRC) were found for the 2PCET mechanism, corresponding to moving along the red curve in Figure 7. Figure 8a shows the energy profile (ΔG^0, kJ mol^{-1}) of the IRC involving the steps (i—iii), where the obtained TS indicates a low activation energy (E_a = 48.6 kJ mol^{-1}) of the 2PCET. Similarly, an energy profile with a TS (E_a = 39.4 kJ mol^{-1}) was obtained using the TPSSh functional (Supporting Information, Figure S8).

Figure 8b demonstrates the relation between the number of electrons in the π-orbital of PiceH$_4$ (blue circles) and the O—H bond distance (3′O—H: red bold line, 4′O—H: red dotted line, nm) along the IRC. The spins were localized on the radicals before and after the TS along the 2PCET, indicating that the radical distributed on O$_2^{\bullet-}$ in the initial PRC was transferred to PiceH$_2^{\bullet-}$ in the PC. The change in the π-electrons of PiceH$_4$ was well correlated with the changes in the spin density distributions on the electron-donor side (PiceH$_4$) and the electron-acceptor side (O$_2^{\bullet-}$). In addition, the TS was electronically characterized by the delocalization of π-electrons over the HB complex (most of the spins were distributed in the O$_2^{\bullet-}$—catechol-stilbene double bond moiety). Consequently, the IRC revealed that a 2PCET from PiceH$_4$ (at the catechol moiety) to O$_2^{\bullet-}$ occurred without generating intermediates—such as HO$_2^{\bullet}$—which is a kinetically superior process in agreement with the electrochemical result. Moreover, the initial PT occurred at 3′OH, forming an intermediate complex (PiceH$_3^-$—HO$_2^{\bullet}$); furthermore, the second PT occurred at 4′OH (para OH) along the 2PCET without dissociation of the HBs. Herein, we compared Figure 8a with the IRC of 2PCET from catechol to O$_2^{\bullet-}$ to elucidate the role of the stilbene moiety of PiceH$_4$. A similar IRC was obtained with a TS for catechol (step (ii)) using both functionals (Supporting Information, Figure S9), where the E_a for PiceH$_4$ (B3LYP:

https://doi.org/10.1021/acsomega.4c01742
ACS Omega 2024, 9, 24889−24898

48.6, TPSSh: 39.4) was lower than that for catechol (52.5, 41.4). Thus, this E_a comparison revealed the kinetically superior $O_2^{\bullet-}$-scavenging ability of $PiceH_4$ compared with that of catechol, implying that the stilbene double bond promotes the 2PCET reaction via the catechol moiety.

These IRC results show that the scavenging of the crystalline form of $O_2^{\bullet-}$ by $PiceH_4$ in DMF is governed by 2PCET at the catechol moiety after the formation of PRC between $PiceH_4$ and $O_2^{\bullet-}$. Notably, the coplanar stilbene moiety kinetically promotes 2PCET at the catechol moiety, where the two rings of $PiceH_4$ linked by the double bond of stilbene expand the π-conjugated plane, demonstrating the successful scavenging of $O_2^{\bullet-}$.

In conclusion, we investigated the reactivities of piceatannol toward electrogenerated $O_2^{\bullet-}$ in DMF. The primary findings are summarized as follows:

1. Piceatannol scavenges $O_2^{\bullet-}$ via the 2PCET mechanism.
2. 2PCET occurs at the catechol moiety of piceatannol.
3. The stilbene moiety of piceatannol promotes the 2PCET.
4. Piceatannol is better $O_2^{\bullet-}/HO_2^{\bullet}$ scavenger compared with *trans*-resveratrol and catechol because of its characteristic structure involving both stilbene and catechol moieties.

These findings primarily concern chemical reactions in aprotic DMF solvents. However, our findings may provide mechanistic insights into the scavenging of $O_2^{\bullet-}$ by $PiceH_4$ in biotic structures, such as lipid bilayers, encouraging the use of $PiceH_4$ as a phytoalexin in human health science.

■ ASSOCIATED CONTENT

Data Availability Statement

T.N., DFT calculations, concerted two-proton-coupled electron transfer (2PCET) between piceatannol and electrogenerated superoxide in *N*,*N*-dimethylformamide, Mendeley Data, V1, 2024, doi: 10.17632/757frcrxnc.1.

Supporting Information

The Supporting Information is available free of charge at https://pubs.acs.org/doi/10.1021/acsomega.4c01742.

CV parameters; in situ controlled-potential electrolytic ESR system; CVs of $PiceH_4$ in the absence of $O_2^{\bullet-}$; CVs with various scan rates; optimized geometries of the compounds; changes in HOMO−LUMO energies; calculated energies and the values; six diabatic electronic states; optimized geometries of the complexes; energy profiles along the reaction coordinates (PDF)

■ AUTHOR INFORMATION

Corresponding Author

Tatsushi Nakayama − *Gifu Pharmaceutical University, Gifu 501-1196, Japan;* orcid.org/0000-0002-0346-2089; Phone: +81-58-230-8100; Email: tnakayama@gifu-pu.ac.jp; Fax: +81-58-230-8200

Author

Bunji Uno − *Gifu University of Medical Science, Gifu 509-0923, Japan;* orcid.org/0000-0003-3844-0362

Complete contact information is available at: https://pubs.acs.org/10.1021/acsomega.4c01742

Funding

This research was funded by the Iwatani Naoji Foundation, Research Foundation for the Electrotechnology of Chubu, Amano Institute of Technology, and Grant-in-Aid for Scientific Research (grant number 19K16338) from the Japan Society for the Promotion of Science.

Notes

The authors declare no competing financial interest.

■ ACKNOWLEDGMENTS

The authors would like to thank Risa Asahara and Yuki Mori for their experimental assistance.

■ ABBREVIATIONS USED

ESR, electron spin resonance; DFT, density functional theory; 2PCET, concerted two-proton-coupled electron transfer; ROS, reactive oxygen species; ET, electron transfer; OH, hydroxyl group; SET, single-electron transfer; HAT, hydrogen-atom transfer; PCET, proton-coupled electron transfer; PT, proton transfer; HB, hydrogen bond; GC, glassy carbon; TS, transition state; HOMO, highest-occupied molecular orbital; LUMO, lowest-unoccupied molecular orbital; PCM, polarized continuum model; NBO, natural bond orbital; CV, cyclic voltammogram; SOMO, singly occupied molecular orbital; PRC, prereactive complex; PC, product complex; IRC, intrinsic reaction coordinate

■ REFERENCES

(1) Navarro, G.; Martínez Pinilla, E.; Ortiz, R.; Noé, V.; Ciudad, C. J.; Franco, R. Resveratrol and Related Stilbenoids, Nutraceutical/Dietary Complements with Health-Promoting Actions: Industrial Production, Safety, and the Search for Mode of Action. *Compr. Rev. Food Sci. Food Saf.* **2018**, *17* (4), 808−826.

(2) Bhat, K. P. L.; Kosmeder, J. W.; Pezzuto, J. M. Biological Effects of Resveratrol. *Antioxid. Redox Signaling* **2001**, *3* (6), 1041−1064.

(3) Münzenberger, B.; Heilemann, J.; Strack, D.; Kottke, I.; Oberwinkler, F. Phenolics of Mycorrhizas and Non-Mycorrhizal Roots of Norway Spruce. *Planta* **1990**, *182* (1), 142−148.

(4) Lee, D.; Cuendet, M.; Schunke Vigo, J.; Graham, J. G.; Cabieses, F.; Fong, H. H. S.; Pezzuto, J. M.; Kinghorn, A. D. A Novel Cyclooxygenase-Inhibitory Stilbenolignan from the Seeds of Aiphanes Aculeata. *Org. Lett.* **2001**, *3* (14), 2169−2171.

(5) Yao, C. S.; Lin, M.; Liu, X.; Wang, Y. H. Stilbene Derivatives from Gnetum Cleistostachyum. *J. Asian Nat. Prod. Res.* **2005**, *7* (2), 131−137.

(6) Geahlen, R. L.; McLaughlin, J. L. Piceatannol (3,4,3′,5′-Tetrahydroxy-Trans-Stilbene) Is a Naturally Occurring Protein-Tyrosine Kinase Inhibitor. *Biochem. Biophys. Res. Commun.* **1989**, *165* (1), 241−245.

(7) Hosoda, R.; Hamada, H.; Uesugi, D.; Iwahara, N.; Nojima, I.; Horio, Y.; Kuno, A. Different Antioxidative and Antiapoptotic Effects of Piceatannol and Resveratrol. *J. Pharmacol. Exp. Ther.* **2021**, *376* (3), 385−396.

(8) Yang, W.; Wang, Y.; Hao, Y.; Wang, Z.; Liu, J.; Wang, J. Piceatannol Alleviate ROS-Mediated PC-12 Cells Damage and Mitochondrial Dysfunction through SIRT3/FOXO3a Signaling Pathway. *J. Food Biochem.* **2022**, *46* (3), No. e13820.

(9) Cordova-Gomez, M.; Galano, A.; Alvarez-Idaboy, J. R. Piceatannol, a Better Peroxyl Radical Scavenger than Resveratrol. *RSC Adv.* **2013**, *3* (43), 20209−20218.

(10) Caruso, F.; Tanski, J.; Villegas-Estrada, A.; Rossi, M. Structural Basis for Antioxidant Activity of Trans-Resveratrol: Ab Initio Calculations and Crystal and Molecular Structure. *J. Agric. Food Chem.* **2004**, *52* (24), 7279−7285.

(11) Gülçin, İ. Antioxidant Properties of Resveratrol: A Structure−Activity Insight. *Innovative Food Sci. Emerging Technol.* **2010**, *11* (1), 210−218.
(12) Qiu, J. M.; Qin, C. F.; Wu, S. G.; Ji, T. Y.; Tang, G. T.; Lei, X. Y.; Cao, X.; Xie, Z. Z. A Novel Salvianolic Acid A Analog with Resveratrol Structure and Its Antioxidant Activities in Vitro and in Vivo. *Drug Dev. Res.* **2021**, *82* (1), 108−114.
(13) Iuga, C.; Raúl Alvarez-Idaboy, J.; Russo, N. Antioxidant Activity of Trans-Resveratrol toward Hydroxyl and Hydroperoxyl Radicals: A Quantum Chemical and Computational Kinetics Study. *J. Org. Chem.* **2012**, *77* (8), 3868−3877.
(14) Storniolo, C. E.; Moreno, J. J. Resveratrol Analogs with Antioxidant Activity Inhibit Intestinal Epithelial Cancer Caco-2 Cell Growth by Modulating Arachidonic Acid Cascade. *J. Agric. Food Chem.* **2019**, *67* (3), 819−828.
(15) Nanni, E. J.; Birge, R. R.; Hubbard, L. M.; Morrison, M. M.; Sawyer, D. T. Oxidation and Dismutation of Superoxide Ion Solutions to Molecular Oxygen. Singlet vs. Triplet State. *Inorg. Chem.* **1981**, *20* (3), 737−741.
(16) Nanni, E. J.; Stallings, M. D.; Sawyer, D. T. Does Superoxide Ion Oxidize Catechol, α-Tocopherol, and Ascorbic Acid by Direct Electron Transfer? *J. Am. Chem. Soc.* **1980**, *102* (13), 4481−4485.
(17) Song, C.; Zhang, J. Electrocatalytic Oxygen Reduction Reaction. In *PEM Fuel Cell Electrocatalysts and Catalyst Layers*; Springer: London, 2008; pp 89−134.
(18) Biela, M.; Rimarčík, J.; Senajová, E.; Kleinová, A.; Klein, E. Antioxidant Action of Deprotonated Flavonoids: Thermodynamics of Sequential Proton-Loss Electron-Transfer. *Phytochemistry* **2020**, *180*, No. 112528.
(19) Singh, P. S.; Evans, D. H. Study of the Electrochemical Reduction of Dioxygen in Acetonitrile in the Presence of Weak Acids. *J. Phys. Chem. B* **2006**, *110*, 637−644.
(20) Weinberg, D. R.; Gagliardi, C. J.; Hull, J. F.; Murphy, C. F.; Kent, C. A.; Westlake, B. C.; Paul, A.; Ess, D. H.; McCafferty, D. G.; Meyer, T. J. Proton-Coupled Electron Transfer. *Chem. Rev.* **2012**, *112* (7), 4016−4093.
(21) Tyburski, R.; Liu, T.; Glover, S. D.; Hammarström, L. Proton-Coupled Electron Transfer Guidelines, Fair and Square. *J. Am. Chem. Soc.* **2021**, *143* (2), 560−576.
(22) Nakayama, T.; Uno, B. Reactivities of Hydroxycinnamic Acid Derivatives Involving Caffeic Acid toward Electrogenerated Superoxide in *N*,*N*-Dimethylformamide. *Electrochem* **2022**, *3* (3), 347−360.
(23) Nakayama, T.; Uno, B. Reactivities of 1,2-, 1,3-, and 1,4-Dihydroxynaphthalenes toward Electrogenerated Superoxide in *N*,*N*-Dimethylformamide through Proton-Coupled Electron Transfer. *Electrochim. Acta* **2022**, *436*, No. 141467.
(24) Nakayama, T.; Uno, B. Concerted Two-Proton-Coupled Electron Transfer from Catechols to Superoxide via Hydrogen Bonds. *Electrochim. Acta* **2016**, *208*, 304−309.
(25) Nakayama, T.; Honda, R.; Kuwata, K.; Usui, S.; Uno, B. Electrochemical and Mechanistic Study of Superoxide Scavenging by Pyrogallol in *N*,*N*-Dimethylformamide through Proton-Coupled Electron Transfer. *Electrochem* **2022**, *3* (1), 115−128.
(26) Nakayama, T.; Uno, B. Reactivity of Trans-Resveratrol toward Electrogenerated Superoxide in N,N-Dimethylformamide. *J. Agric. Food Chem.* **2023**, *71* (10), 4382−4393.
(27) Leonard, S. S.; Xia, C.; Jiang, B. H.; Stinefelt, B.; Klandorf, H.; Harris, G. K.; Shi, X. Resveratrol Scavenges Reactive Oxygen Species and Effects Radical-Induced Cellular Responses. *Biochem. Biophys. Res. Commun.* **2003**, *309* (4), 1017−1026.
(28) Li, D.-D.; Han, R.-M.; Liang, R.; Chen, C.-H.; Lai, W.; Zhang, J.-P.; Skibsted, L. H. Hydroxyl Radical Reaction with Trans-Resveratrol: Initial Carbon Radical Adduct Formation Followed by Rearrangement to Phenoxyl Radical. *J. Phys. Chem. B* **2012**, *116* (24), 7154−7161.
(29) Shang, Y.-J.; Qian, Y.-P.; Liu, X.-D.; Dai, F.; Shang, X.-L.; Jia, W.-Q.; Liu, Q.; Fang, J.-G.; Zhou, B. Radical-Scavenging Activity and Mechanism of Resveratrol-Oriented Analogues: Influence of the Solvent, Radical, and Substitution. *J. Org. Chem.* **2009**, *74* (14), 5025−5031.
(30) Okumura, N.; Uno, B. Electronic Spectra of the Electrogenerated 1,4-Benzoquinone π-Dianion and the Strongly Hydrogen-Bonded Charge-Transfer Complex with Methanol. *Bull. Chem. Soc. Jpn.* **1999**, *72* (6), 1213−1217.
(31) Zhao, Y.; Truhlar, D. G. The M06 Suite of Density Functionals for Main Group Thermochemistry, Thermochemical Kinetics, Noncovalent Interactions, Excited States, and Transition Elements: Two New Functionals and Systematic Testing of Four M06-Class Functionals and 12 Other Function. *Theor. Chem. Acc.* **2008**, *120* (1−3), 215−241.
(32) Jensen, K. P. Bioinorganic Chemistry Modeled with the TPSSh Density Functional. *Inorg. Chem.* **2008**, *47* (22), 10357−10365.
(33) Perdew, J. P.; Tao, J.; Staroverov, V. N.; Scuseria, G. E. Meta-Generalized Gradient Approximation: Explanation of a Realistic Nonempirical Density Functional. *J. Chem. Phys.* **2004**, *120* (15), 6898−6911.
(34) Frisch, M. J.; Trucks, G. W.; Schlegel, H. B.; Scuseria, G. E.; Robb, M. A.; Cheeseman, J. R.; Scalmani, G.; Barone, V.; Petersson, G. A.; Nakatsuji, H.; Li, X.; Caricato, M.; Marenich, A. V.; Bloino, J.; Janesko, B. G.; Gomperts, R.; Mennucci, B.; Hratchian, H. P.; Ortiz, J. V.; Izmaylov, A. F.; Sonnenberg, J. L.; Williams-Young, D.; Ding, F.; Lipparini, F.; Egidi, F.; Goings, J.; Peng, B.; Petrone, A.; Henderson, T.; Ranasinghe, D.; Zakrzewski, V. G.; Gao, J.; Rega, N.; Zheng, G.; Liang, W.; Hada, M.; Ehara, M.; Toyota, K.; Fukuda, R.; Hasegawa, J.; Ishida, M.; Nakajima, T.; Honda, Y.; Kitao, O.; Nakai, H.; Vreven, T.; Throssell, K.; Montgomery, J. A., Jr.; Peralta, J. E.; Ogliaro, F.; Bearpark, M. J.; Heyd, J. J.; Brothers, E. N.; Kudin, K. N.; Staroverov, V. N.; Keith, T. A.; Kobayashi, R.; Normand, J.; Raghavachari, K.; Rendell, A. P.; Burant, J. C.; Iyengar, S. S.; Tomasi, J.; Cossi, M.; Millam, J. M.; Klene, M.; Adamo, C.; Cammi, R.; Ochterski, J. W.; Martin, R. L.; Morokuma, K.; Farkas, O.; Foresman, J. B.; Fox, D. J.. *Gaussian 16*, revision B.01; Gaussian Inc.: Wallingford, CT, USA, 2016.
(35) Kremleva, A.; Aparicio, P. A.; Genest, A.; Rösch, N. Quantum Chemical Modeling of Tri-Mn-Substituted W-Based Keggin Polyoxoanions. *Electrochim. Acta* **2017**, *231*, 659−669.
(36) Quintero-Saumeth, J.; Rincón, D. A.; Doerr, M.; Daza, M. C. Concerted Double Proton-Transfer Electron-Transfer between Catechol and Superoxide Radical Anion. *Phys. Chem. Chem. Phys.* **2017**, *19* (38), 26179−26190.
(37) Reed, A. E.; Weinstock, R. B.; Weinhold, F. Natural Population Analysis. *J. Chem. Phys.* **1985**, *83* (2), 735−746.

https://doi.org/10.1021/acsomega.4c01742
ACS Omega 2024, 9, 24889−24898